Hindawi Publishing Corporation
Advances in Tribology
Volume 2008, Article ID 561280, 10 pages
doi:10.1155/2008/561280

Research Article

Experimental Investigation into the Tractive Prerolling Behavior of Balls in V-Grooved Tracks

Kris De Moerlooze and Farid Al-Bender

Mechanical Engineering Department, Division PMA, Katholieke Universiteit Leuven, Celestijnenlaan 300B, 3001 Heverlee, Belgium

Correspondence should be addressed to Farid Al-Bender, farid.al-bender@mech.kuleuven.be

Received 19 September 2007; Revised 8 January 2008; Accepted 27 February 2008

Recommended by Farshid Sadeghi

In a rolling element system, the period of transition between motion commencement and the attainment of steady state, gross rolling, and termed prerolling is of common concern to many engineering applications. This region is marked by hysteresis friction behavior, with a characteristic friction-displacement curve, which is in particular relevant to motion characterization and control issues. In a previous paper, the authors carried out a theoretical analysis of tractive prerolling, leading to a model for simulating this phenomenon. The present paper is dedicated to the experimental investigation of tractive prerolling friction behavior, including validation of the theoretical model. Firstly, a kinematic analysis of the rolling motion in V-grooved tracks is carried out. Secondly, the influence of the normal load on the frictional behavior, in prerolling up to the attainment of gross rolling, is investigated on a dedicated test setup. Finally, the newly developed theoretical model is validated by comparison with the experimental results. Satisfactory agreement is obtained between theory and experiment.

1. INTRODUCTION

The characterization of rolling friction is a pertinent issue in many fields ranging from rolling stock, aircraft servo systems, and rotary and linear positioning systems to the control of miniature reading/writing heads, friction drives, and high precision systems. This topic has therefore been gaining importance over the last decades, owing to the increasing demands of industrial applications on positioning accuracy, wear, and controllability. A common concern in all these applications is the rolling element system's behavior between motion reversal points, in other words, the period between motion commencement and the attainment of gross rolling. This period is referred to as prerolling, which is akin to presliding in sliding contacts [1–3]. Prerolling is marked by a clear hysteresis behavior with nonlocal memory, which lies at the root of the strongly nonlinear dynamic behavior that characterizes systems comprising rolling elements [4, 5]. The design parameters of rolling element systems, such as preload, ball diameter, and track groove angle, evidently, have their influence on the frictional behavior of the system. Despite this fact, a coherent, systematic theory that correlates behavior with parameters has not yet received the attention it deserves in the literature, owing to many reasons, in particular the complexity and the strong nonlinearity of the rolling contact problem.

Rolling resistance or, as it is often called, rolling friction arises from two basic mechanisms: internal mechanical losses in the bulk of rolling objects and external tractions in the rolling contact patch. In case of elastic rolling objects (such as metallic objects), the former is generally negligible in magnitude in comparison with the latter. This paper is concerned with tractive rolling; more specifically that, which is caused by creepages in the rolling motion, in particular, spin creepage.

When an elastic body of revolution rolls tractively over another, the traction field in the contact patch changes progressively with the distance traversed from its initial distribution until it reaches a certain steady-state distribution. This distribution, which is independent of the initial field prior to commencement of rolling, does not vary with further rolling. This eventual rolling regime is termed gross rolling; the period building up to it, from commencement of rolling, is termed the prerolling regime. The resultant

traction in this regime is characterized by rate-independent hysteresis behavior with nonlocal memory in function of the traversed displacement [2]. In this reference, an extensive experimental study of prerolling behavior of a ball in V-groove application has been reported, where the reader may also find a short overview of literature around the subject. The conclusions and correlations presented in that study remained, however, empirical.

Recently, the present authors have developed a theoretical model, which is able to simulate tractive prerolling (and transition to gross rolling) in an arbitrary rolling contact [6]. The present paper introduces on the one hand an experimental validation of that model and on the other hand a check of the validity of Amontons' law as applied to rolling contacts.

Bearings can be considered as one of the most important machine elements in regard to accuracy of motion. However, only few types of bearings, notably cylindrical and tapered roller bearings, contain rolling elements which undergo pure rolling, that is, rolling without creepage, which leads to microslip. In other types, such as pivot bearings, axially loaded deep groove ball bearings, angular contact bearings, and recirculating rolling element guideways, the rolling motion of the rolling elements comprises a significant amount of microslip which in those cases is responsible for the greatest part of the frictional losses. This microslip depends on the relative velocity (or creepage) between the contacting surfaces and on the elasticity.

Other applications where rolling with creepage appears are gears and friction wheel transmissions. The study of rolling contacts comprising microslip becomes therefore an important research issue.

Compared to steady state rolling friction, only a few experimental studies in the field of prerolling have been conducted. Liu et al. [7] perform some experiments on a newly developed test apparatus in this field. They distinguish three regimes for the coefficient of rolling friction, namely, a gradually increasing coefficient in the elastic deformation regime, a peak in the transition zone, and a constant value in the gross rolling regime. Additionally, the wear behavior of steel is investigated under different conditions. The breakaway rolling friction (i.e., the peak value prior to commencement of gross rolling) is studied by Budinski [8] in a case study in which he presents a modified test procedure for the breakaway coefficient of rolling friction for rolling element bearings.

Endo et al. [9] study the nonlinear spring characteristic of a rolling element in the transient zone. They link the energy losses in the contact to the overall damping characteristics of the rolling system and confirm experimentally that these losses vary when rolling elements with different diameters are used. Otsuka and Masuda [10] call the prerolling region the "nonlinear spring area" and try to explain the influence of the nonlinear spring behavior (NSB) on the frequency response in some practical case studies.

Besides dry rolling contacts, lubricated contacts have also been investigated in the past. Wang et al. [11] investigate the behavior of EHL films under pure rolling, short stroke reciprocating motion. High-speed color camera measurements are compared to simulations with multigrid techniques.

Xiao et al. [12] have suggested a friction model for dry and lubricated rolling of rough bodies. They observe a linear increasing coefficient of rolling friction with increasing mean contact pressure, up to a maximum limit above which the coefficient of friction stays constant.

Load variations in mechanical systems comprising rolling elements often occur, while their influence on the frictional behavior is neglected in control models. This may impose a limit on the attainable positioning accuracy. Since this issue is of importance in machine design and control, this study deals with the influence of the normal load on the prerolling behavior. The first objective is to verify the effect of the normal load on the overall shape and behavior of the hysteresis loop on an existing test setup. The second objective is the verification of the theory presented in [6] (which is the theoretical part of this study) for the case of rolling with spin creepage.

The paper is organized as follows. Section 2 considers the kinematics of the rolling element system which is used during the experiments and estimates the relative order of magnitude of the various types of possible friction losses. Section 3 gives an overview of the experiments. In Section 4, the hysteresis identification is discussed. A model equation is proposed which is used to fit and process the data for further analysis. In Section 5, the influence of the normal load on the parameters of the model equation is studied. All these aspects provide the prerequisites for the validation of the theoretical model, presented in [6], in Section 6. Finally, appropriate conclusions are drawn and future work is outlined.

2. ANALYSIS OF ROLLING FRICTION FOR A BALL IN A V-GROOVED TRACK

As mentioned in the previous section, rolling friction may be caused by internal losses and/or external tractions. Consequently, it may be pertinent to gain some idea of the mechanisms, parameters, and orders of magnitudes of any possible mechanism prior to embarkation on a test program. In this section, we first examine the kinematics of motion of the ball in order to evaluate the creepages associated with that motion. Secondly, we assess the importance of each rolling friction mechanism.

2.1. Kinematics of a ball rolling in V-grooved tracks

As mentioned in the introduction, the tractive rolling subject of this investigation arises mainly as a consequence of creepages imposed on the otherwise pure rolling motion. For a formal definition of the principal creepages, the reader is referred to [6]. In the case of balls rolling between two V-grooved tracks, the most dominant type of creepage is spin. Quantification of relative spin, that is, the amount of spin per unit rolling distance is therefore essential for evaluating tractive friction. To this end, this section presents a kinematic analysis of the motion of the balls between the V-grooves.

Consider a ball rolling between two V-grooved tracks as depicted in Figure 1. When the lower track moves, with a

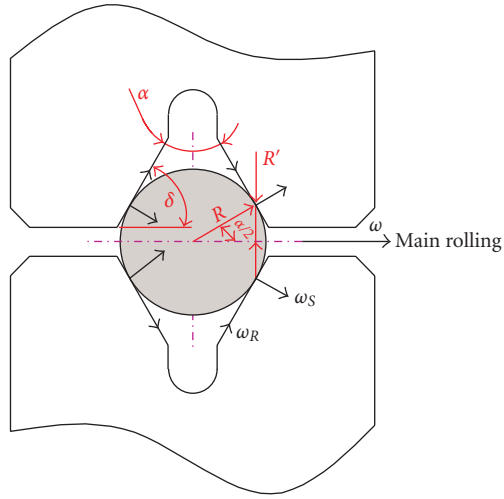

Figure 1: The roll and spin motion.

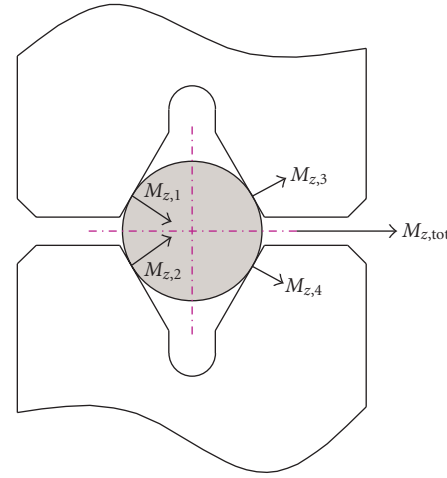

Figure 2: The local spin moments result in a global spin moment $M_{z,\text{tot}}$.

velocity V normal to the plane of the page, the ball will roll between the grooves with a main rolling velocity ω. This latter may be resolved into a pure rolling motion ω_R and a pure spin motion ω_S. In the case of pure rolling, the creepage is assumed zero, thus no microslip takes place. In other words, for the case of a ball in the V-grooved tracks, the spin component of the rolling motion is the only creepage responsible for the frictional losses. As a consequence, the friction resistance will increase with decreasing groove angle, as the spin per unit rolling increases with a decreasing groove angle. The other limiting case is the rolling of a sphere in between two horizontal flat plates, where consequently no creepage occurs. In this case, the only remaining sources of rolling friction are elastic hysteresis losses and Heathcote slip (see further below).

A linear motion of the lower V-groove corresponds to a main angular velocity ω:

$$\omega = \frac{V}{R'}, \tag{1}$$

with R' being the distance depicted in Figure 1. This main motion can be resolved into a pure rolling motion ω_R and a pure spin motion ω_S:

$$\begin{aligned} \omega_R &= \omega\cos(\delta) = \omega\sin\left(\frac{\alpha}{2}\right), \\ \omega_S &= \omega\sin(\delta) = \omega\cos\left(\frac{\alpha}{2}\right), \end{aligned} \tag{2}$$

thus,

$$\begin{aligned} R' &= R\sin\left(\frac{\alpha}{2}\right), \\ \omega_S &= \frac{V\cos(\alpha/2)}{R\sin(\alpha/2)}, \\ \omega_R &= \frac{V}{R}. \end{aligned} \tag{3}$$

2.2. Rolling friction forces

Beginning with the traction forces, let us note that the forces associated with the kinematics outlined above may be obtained in an analogous way. Thus, let the motion of the sphere result in a spinning moment M_z, at each contact patch, which gives rise to the frictional force that has to be overcome by the linear actuator. For one ball, four spin components M_z are formed, as depicted in Figure 2, which result in a global spin moment $M_{z,\text{tot}}$, around the rolling axis, that is given by

$$M_{z,\text{tot}} = 4M_z\cos\left(\frac{\alpha}{2}\right). \tag{4}$$

The rolling friction force, per ball, associated with this moment is given by

$$F_{\text{fric,tot}} = \frac{4M_z\cos(\alpha/2)}{2R'} = \frac{2M_z\cos(\alpha/2)}{R\sin(\alpha/2)}. \tag{5}$$

Thus, the coefficient of rolling friction owing to tractive rolling is given by

$$\lambda_{\text{tractive}} = \frac{F_{\text{fric}}}{W} = \frac{M_{z,\text{tot}}}{WR\sin(\alpha/2)}, \tag{6}$$

with W the externally applied normal load.

We turn our attention presently to the other two phenomena responsible for the measured friction in experiments, namely, bulk elastic hysteresis and Heathcote slip.

Firstly, rolling resistance as a consequence of the elastic hysteresis losses due to Hertzian compression is given by [13]

$$\lambda_{\text{elastic}} = \frac{3\epsilon a}{16R}, \tag{7}$$

where ϵ is the coefficient of elastic hysteresis loss due to Hertzian compression and a is the radius of the contact patch which is given by

$$a = \left(\frac{3}{4}\frac{WR}{E^*}\right)^{1/3}. \tag{8}$$

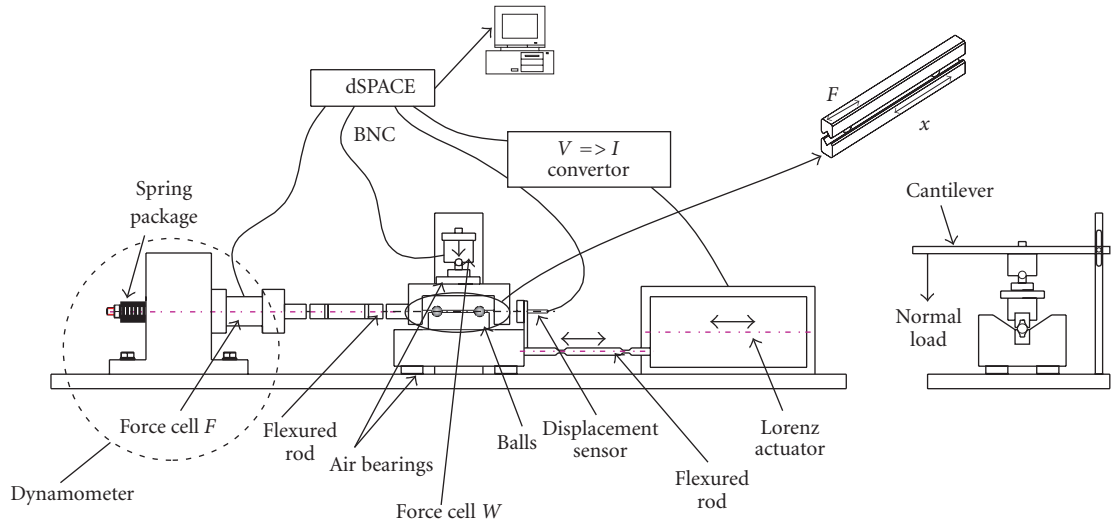

Figure 3: A schematic overview of the tribometer.

Secondly, Heathcote [14] deduced a formulation for the frictional moment M for the case of pure rolling by neglecting the elastic compliance of the contacting bodies [15],

$$\frac{M}{W} = 0.08\mu\frac{a^2}{R}, \tag{9}$$

with μ being the local coefficient of sliding friction. From this equation, one can derive an expression for the coefficient of rolling resistance due to Heathcote slip,

$$\lambda_{\mathrm{HC}} = \frac{M}{RW} = 0.08\frac{\mu a^2}{R^2}. \tag{10}$$

2.3. Order of magnitude analysis

The three phenomena together (6), (7), and (10) account for the total coefficient of rolling friction measured in the subsequently presented experiments. It is thus interesting to gauge the relative importance of these different rolling friction contributions in the context of our experiments.

Thus, let us consider a steel ball of 6 mm diameter, a maximal load W of 20 N and a coefficient of sliding friction μ of 0.5. The contact radius a will be on the order of 10^{-4} m. Experiments reported in this paper show a rolling friction value on the order of 10^{-2}. Considering a realistic coefficient of elastic hysteresis loss ϵ of 0.01, the coefficient of rolling friction due to elastic hysteresis losses $\lambda_{\mathrm{elastic}}$ is on the order of 10^{-5}. The coefficient of rolling friction due to Heathcote slip λ_{HC} is on the order of 10^{-8}.

This estimation indicates that the contribution of traction (in this case, microslip associated with the spin creepage) is by far the most dominant, compared to the two other energy dissipating phenomena.

3. OVERVIEW OF THE EXPERIMENTS

3.1. The test setup

The experimental investigation is carried out on a previously developed tribometer (we refer to [3] for more details) with some minor adaptations. Figure 3 depicts a schematic view of the setup. The tribometer comprises four parts. (1) the actuator part is fixed to the base plate. It comprises a Lorenz actuator, which drives the lower friction member through a flexured rod. (2) The frictional part contains (i) the lower friction member, which in our case is the lower V-track mounted to a block that floats on air bearings and is driven by the aforementioned actuator, and (ii) the upper friction member which is the upper V-track, being connected to the dynamometer via an elastic hinge; (3) a normal loading part, which comprises a cantilever to apply the load through an air bearing; and (4) the sensor part which comprises (i) a Bently eddy current sensor which measures the relative motion between the two friction members, (ii) the friction force dynamometer which contains a force cell attached to a fixed frame that is fixed to the base plate, and (iii) a force cell for measuring the normal load. These different parts are decoupled as far as possible. The Lorenz actuator imposes a straight motion, with a periodic velocity, to the lower friction member through the flexured rod. The Lorenz actuator is current driven and the position signal of the displacement sensor is used for feedback control to obtain, as best as possible, the desired motion of the moving part.

The purpose of the employed elastic joints is to set off alignment errors of the friction block in the normal, lateral, and rotational directions.

The loading part allows easy control of the normal load on the frictional part. The load is applied by using a cantilever (see Figure 3) and is transmitted to the frictional part through an air bearing, in order to avoid affecting the

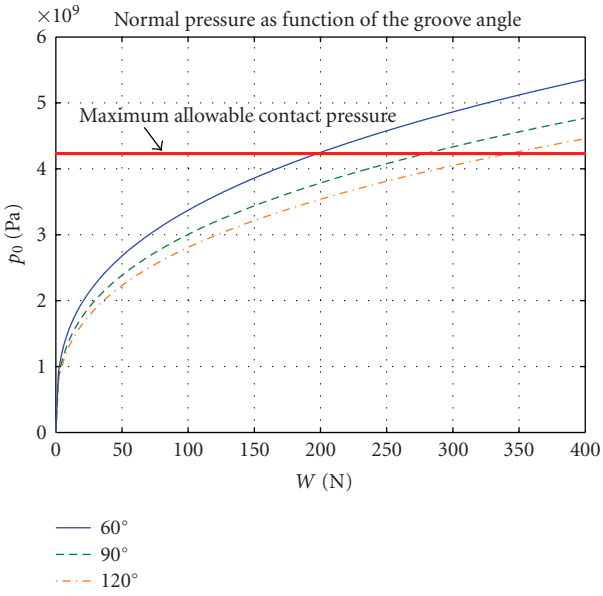

Figure 4: Determination of the maximum allowable normal load (6.35 mm steel balls).

inertia of the frictional part when changing the normal load (mass). Another advantage of the air bearing is that the load is applied without direct contact which may introduce adventitious forces. The air bearing is equipped with a ball joint to allow the bearing to adapt its orientation with respect to the friction block. In this way, a uniform load is applied normal to the friction contact. Detailed experimental characterization of this setup can be found in [16].

3.2. The normal load limitations

In order to guarantee the applicability of Hertz's theory and the elastic behavior of the contacting bodies, the maximum allowable load is calculated. From the work of Tabor [17], plasticity first occurs when the Hertzian contact pressure reaches the limit of approximately $0.6H$, where H is the hardness. Thus for a circular contact,

$$p_0 = \frac{1}{\pi}\left(\frac{6WE^{*2}}{R^2}\right)^{1/3} < 0.6H. \tag{11}$$

In Figure 4, the evolution of the contact pressure is depicted as function of the normal load on the V-grooved track for different opening angles of the V grooves and the case of two steel balls of diameter 6.35 mm. For the used V groove of 60°, the maximum applicable load approximates to 200 N. For higher loads, the *brinelling* effect occurs which means that plastic damage of the contacting surfaces takes place.

3.3. Measurement procedure

For the purpose of this study, the displacement of the moving block and the friction force are measured by the sensors described above and captured using a dSPACE system. To improve the quality of the measured data, a lowpass filter with a bandwidth of 30 Hz is used to exclude most of the measurement noise. The filter is applied to all channels in the same way in order to avoid phase shift effects. Afterwards, the data samples, obtained from repeated test runs for any single test condition, are time averaged to remove random noise and to improve their statistical relevance.

4. IDENTIFICATION OF PREROLLING HYSTERESIS

The aim of the measurements is to evaluate the prerolling behavior of the friction force for different normal loads. The prerolling friction force is function of the displacement which can be described by a rate-independent hysteresis function. The hysteresis curve is fully determined by its *virgin curve* (see [18] for detail). This theoretical curve starts at the origin (with the very first commencement of motion) has positive first and second derivatives for all displacements, and saturates for large displacements. Therefore, it is interesting to use the virgin curve as reference for comparing the hysteresis curves for the different experiments, since this curve incorporates all information of the hysteresis behavior. Once a hysteresis loop is identified, one can determine the virgin curve by scaling the identified curve, by factor 2 in both x and y directions, and shifting the turning points to the origin [18].

A measured hysteresis curve is identified by fitting it to a parametric model using nonlinear regression, in order to capture the curve in a mathematical form. In this study, a two parameter model is chosen for simplicity which is of the form

$$F(x) = h_0\left(1 - e^{-a(x-x_0)}\right). \tag{12}$$

The parameter h_0 gives the saturation value of the curve, while the parameter a is a measure of the curvature. Finally, the parameter x_0 is necessary for the translation along the x-axis. For other suitable model equations, we refer to [2].

Figure 5 shows an example of the model equation fitted to measured hysteresis data. Both the external loop and the derived virgin curve are depicted.

5. INFLUENCE OF THE NORMAL LOAD

Examples of the fitted virgin curves for the different normal loads are visualized in Figure 6. The determining parameters for these curves are h_0 and a which are depicted in Figures 7(a) and 7(b). One can observe an increasing trend for h_0 as function of the external normal load W, while the curvature a as function of the external normal load W shows a decreasing trend. Both trends can be fitted by a linear equation, as shown in the figures. The range of performed experiments result in a spread of h_0 of approximately factor 3 (between minimum and maximum values), while the results for parameter a give a spread of approximately a factor of 1.1. For the sake of gaining an idea about the shape deviations, let us take a to be fixed to a value equal to its mean value of 0.0325. In that case, the error on a approximates to ±5%. In this study however, the parameter a is considered to have a linear decreasing trend as function of the normal load W

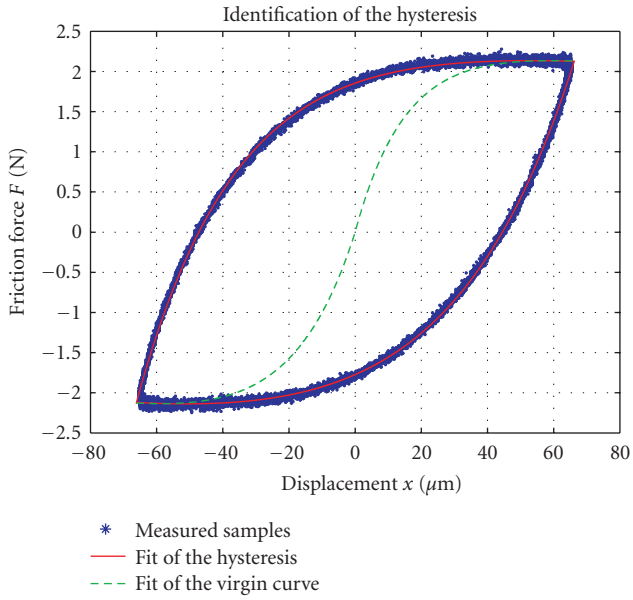

Figure 5: Identification of the hysteresis loop, including the determination of the virgin curves. (Steel balls ϕ6.35 mm, groove angle: 60°, $W = 88.9$ N).

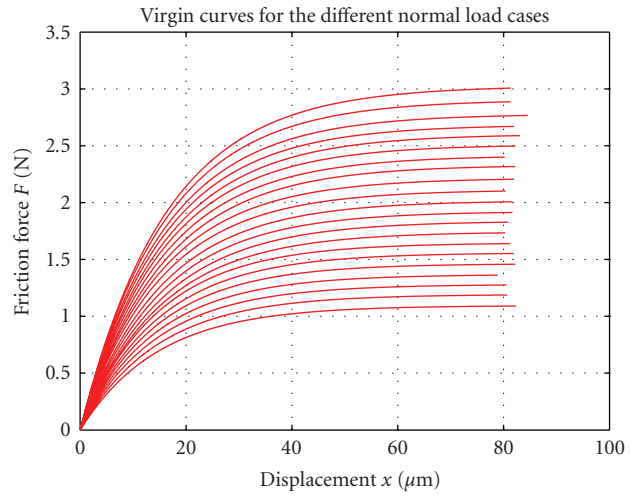

Figure 6: The identified virgin curves for the different normal load cases (46.5 N $\leq W \leq$ 123.2 N).

which reduces the error further to approximately 3%. In other words, the effect of the normal load on the shape of the hysteresis curve is not appreciable.

In Figure 8, the virgin curves are scaled by the applied normal load to obtain the evolution of $\lambda = F/W$, the coefficient of rolling friction. One can observe a slightly increasing trend for λ in function of the external normal load.

In order to ascertain the influence of sliding friction characteristics (of the ball/guideway surfaces) on the rolling friction values, experiments with other ball types are carried out on the same setup. Balls of diameter of 6 mm, coated with a thin layer of diamond-like carbon, are compared to the former uncoated steel balls. The results are depicted in Figure 9. While the same general trends are visualized for these DLC coated balls, one can notice the appreciably lower rolling friction values (by factor 0.3) for the coated balls. This confirms our previous conclusion (see Section 2.2) that the greatest part of the rolling resistance, for this bearing configuration, is owing to microslip tractions and not to elastic hysteresis in the ball/groove material. Furthermore, for the DLC-coated balls, the spread of the parameter h_0 approximates to a factor of 2.8. As for the parameter a, the error committed by taking it as a constant (equal to 0.125), is ±12%, while considering the linear decreasing trend reduces the error to approximately 1%.

6. COMPARISON BETWEEN MODEL AND EXPERIMENT

The second aim of this article is the validation of a theoretical model presented in [6]. The model is able to predict creepage induced traction during and after prerolling.

For the sake of completeness, a short overview of the model is given in the next section. Afterwards, the model is validated by means of the previously presented experimental results for the case of rolling with spin.

6.1. Overview of the model structure [6]

For rolling objects, the relative rigid motion of the counter surfaces termed the creepage, **C**, which consists of longitudinal and lateral creepages, and spin. The (elastic) surface displacement field, **u**, is related to the slip field, **S**, by the equation

$$\mathbf{S} = \mathbf{C} - \frac{\partial \mathbf{u}}{\partial x} + \frac{\partial \mathbf{u}}{\partial q}, \tag{13}$$

Analysis for the case of no slip results in closed form expression for the displacement of the surface particles:

$$\mathbf{u} = f(\mathbf{C}, x, y, q), \tag{14}$$

where x, y are the coordinates of the points in the contact patch, and q is the traversed rolling distance.

To take slip into consideration, the newly obtained values $\mathbf{u} = (u, v)$ are used to calculate the pressure distribution in the contact patch:

$$(p_x, p_y) = L(u, v). \tag{15}$$

If $\|(p_x, p_y)\| \leq \mu p_z$, no slip occurs ($S_x = S_y = 0$) and the values of (u, v) are retained. In the other case, $\|(p_x, p_y)\| > \mu p_z$, the no slip deformation is replaced by

$$(u, v)_{\text{new}} = \frac{\mu p_z}{L} \left(\frac{(u, v)}{\|(u, v)\|} \right)_{\text{old}}. \tag{16}$$

Finally, the traction forces and spin moment are calculated as follows:

$$\begin{aligned} (F_x, F_y) &= \int_{-a}^{a} \int_{-a(y)}^{a(y)} (p_x, p_y)\, dx\, dy, \\ M_z &= \int_{-a}^{a} \int_{-a(y)}^{a(y)} p(x, y) r(x, y)\, dx\, dy. \end{aligned} \tag{17}$$

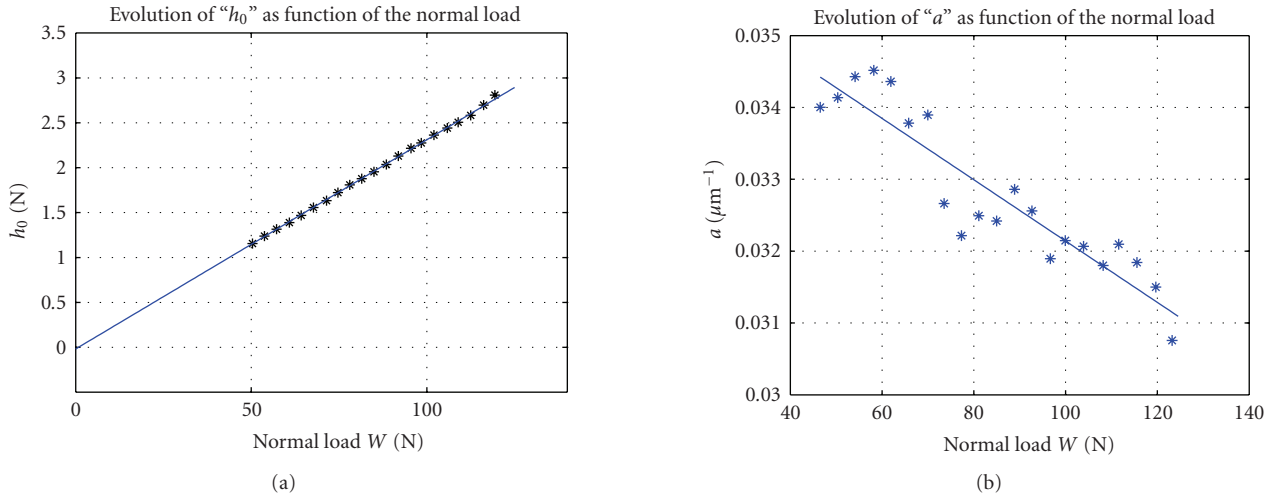

Figure 7: The evolution of h_0 (a) and a (b) with the normal load.

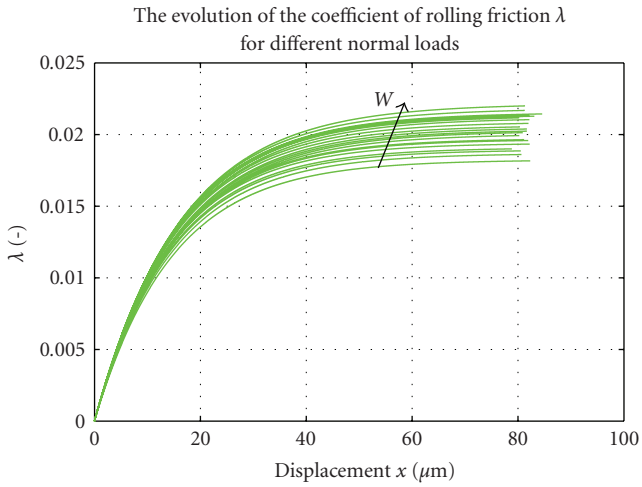

Figure 8: The evolution of λ with the normal load.

In order to calculate the tractions using this model, one needs to know (i) the geometry and elastic properties of the rolling objects, (ii) the normal load, (iii) the creepages, and (iv) the local sliding friction coefficient in the contact. From the kinematics of a V-grooved setup, it appears that only spin creepage is present. Furthermore, only the spin moments are of interest, since the force in the rolling direction F_x equals zero for every contact patch, and the force, F_y, perpendicular to the rolling direction will have a resultant that is equal to zero when taking all four contact patches into consideration.

6.2. Experimental validation of the model

To validate the model, presented in [6], the experimental results are compared to the model predictions. The model is implemented for the kinematics of the V-grooved track, using reasonable values for the elastic parameters. The local coefficient of sliding friction, necessary for the model, is determined by an additional experiment. In this experiment, the coefficient of sliding friction is determined for the system of a ball on the track as sliding counter surface. This is carried out by gluing two balls on a plate, and using this as counter surface for one of the V-grooves. Periodic sliding motion is imposed for different normal loads, while the friction force is measured. The coefficient of sliding friction is determined by dividing the measured friction force by the applied normal load. Although this rudimentary experiment ignores some basic rules as, for example, the velocity dependence of the coefficient of friction; these estimates are accurate enough for a first evaluation of the model and are a good starting point for further analysis. Note that, Lampaert et al. [3] show that the velocity dependence of the coefficient of friction for metallic contacts is small. The sliding friction results of this experiment are depicted in Figure 10 for different normal loads. The results of this short experiment are used as input for the model.

The experimentally obtained virgin curves of Section 4 are now compared with the model results in Figure 11. We note a good resemblance between model and experimental results. The initial slope as well as the saturation value behave in ways similar to theoretical predictions.

In Figure 12, the error, according to (18) below, between model and experiment is presented for the different virgin curves. For clarity, only a few characteristic results are presented. The error is defined as follows:

$$\text{error} = \frac{\left|\left(F_{\text{measured}} - F_{\text{model}}\right)\right|}{F_{\text{mean}}}, \tag{18}$$

where $F_{\text{mean}} = (F_{\text{measured}} + F_{\text{model}})/2$, calculated as function of the displacement.

In Figure 13, for every virgin curve, the error is averaged and divided by the maximum friction force. One can distinguish two regions. Firstly, experiments with high normal loads show an error lying within 5%. Secondly, experiments with small normal loads show an error lying in the range of 6–16%. An obvious explanation to this is the smaller signals and thus the lower signal-to-noise ratio of those experiments.

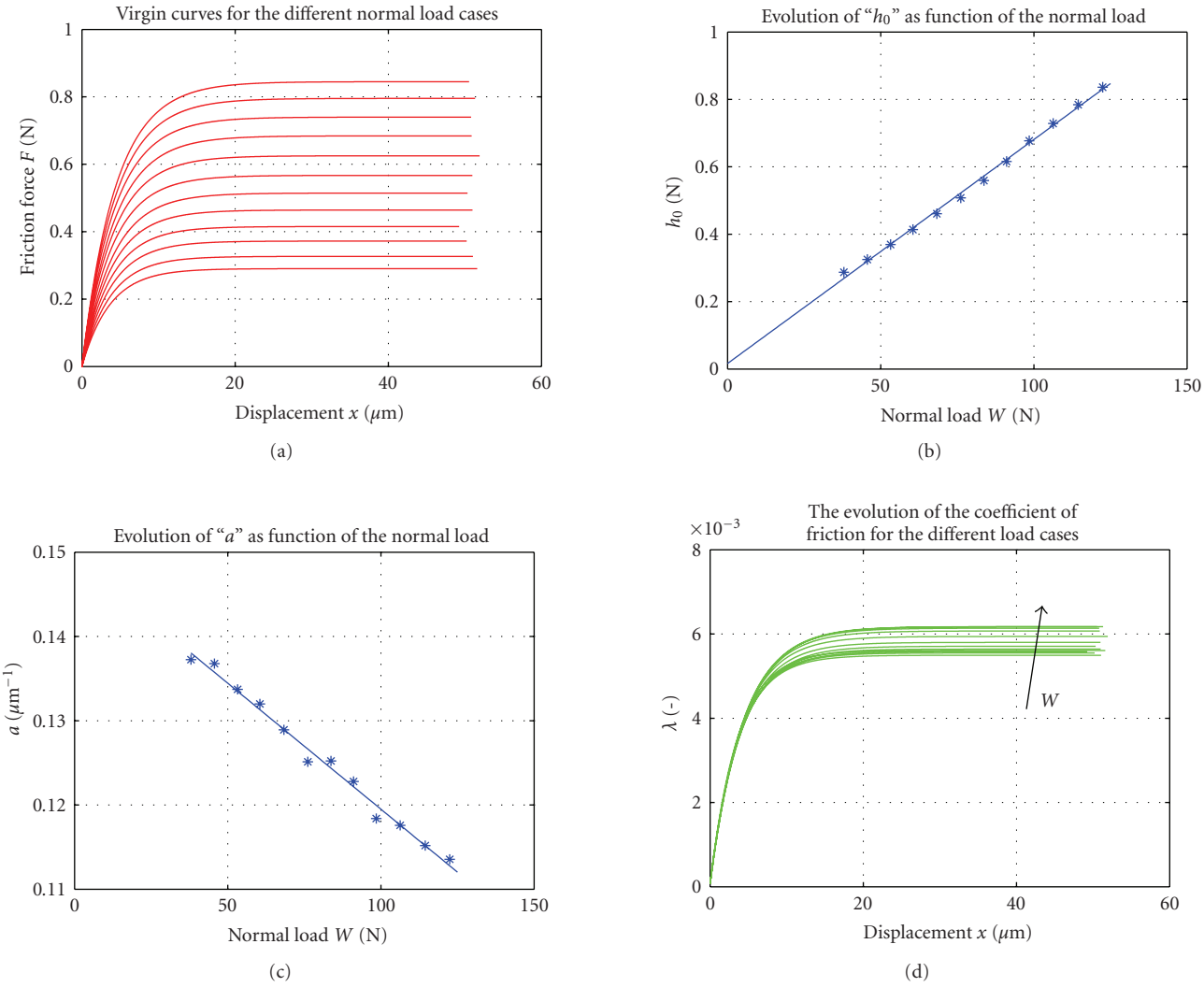

Figure 9: Results for the diamond coated balls (ϕ6 mm, 60° opening angle).

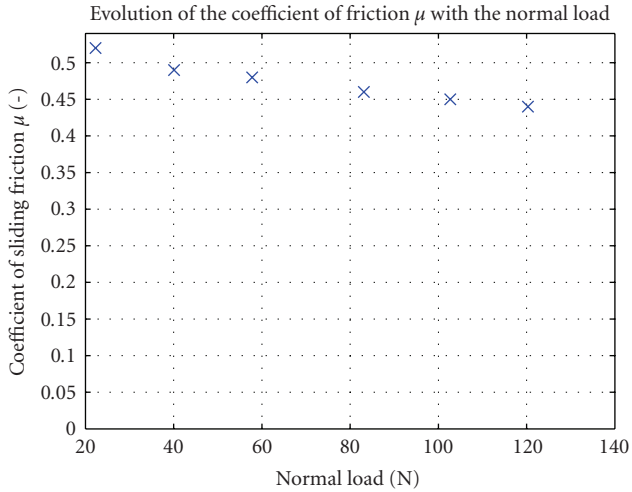

Figure 10: The evolution of the coefficient of sliding friction as function of the normal load.

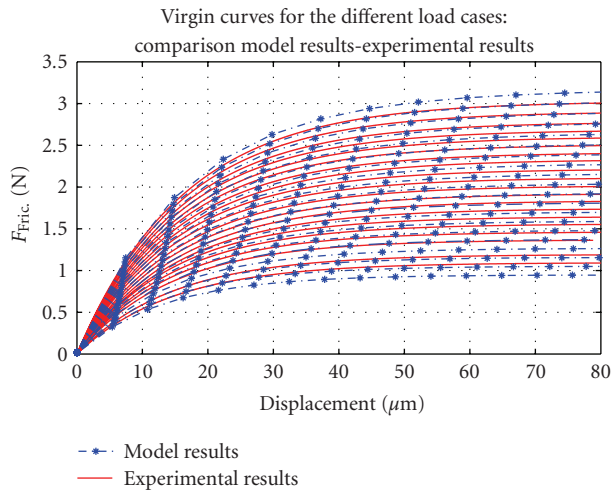

Figure 11: A comparison between experimental results and model results of [6] (6.35 mm steel balls, 60° groove angle, 46.5 N $\leq W \leq$ 123.2 N).

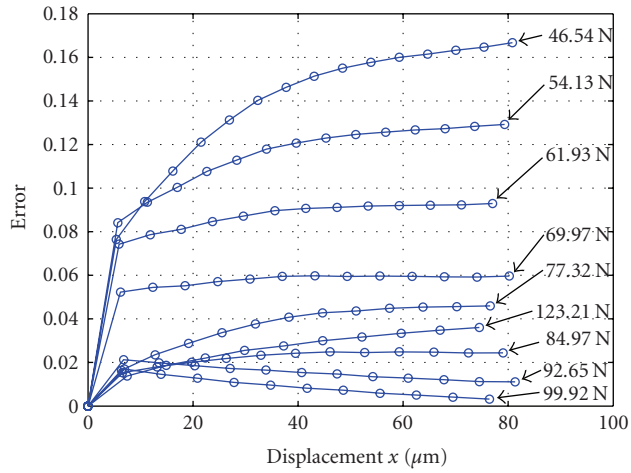

Figure 12: The error between model and experimental results.

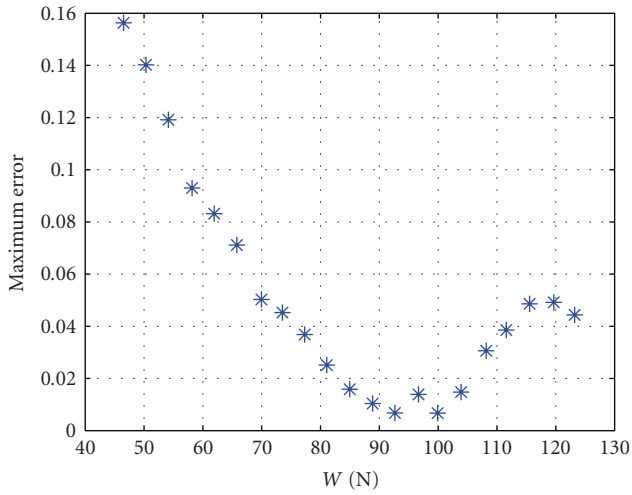

Figure 13: The maximum error between model and experimental results as function of the normal load.

7. DISCUSSION AND CONCLUSIONS

In this paper, an experimental investigation of prerolling is presented. More specifically, the influence of the normal load on the hysteresis behavior is studied on an existing setup, in which the frictional element comprises two balls rolling between a pair of V-grooved tracks. The frictional hysteresis is fitted by an exponential model form, in which two parameters characterize the shape, denoted by the curvature, and the saturation value of the friction force, respectively. The evolution of these parameters as function of the normal load is presented. We observe a slight increase in the coefficient of rolling friction λ with an increasing normal load and a very small change in the curvature.

Another part of the investigation carries out a validation of an existing theoretical model for tractive rolling by use of the obtained experimental data. Kinematic analysis of a rolling configuration shows that the only creepage present is spin. Using the experimentally determined sliding friction coefficient and spin values as input to the model, a comparison of model prediction and experiment is carried out. Agreement between model and experiment falls within an error margin of less than 16% for low normal loads and 5% for high normal loads.

8. FUTURE WORK

The global aim of this experimental research is the determination of the relation between the hysteretic friction force and the different system parameters. In [2], Al-Bender and Symens investigate other system parameters as groove angle, ball diameter, and so forth. A global synthesis of these results, together with the results of this study, can improve the understanding of the frictional behavior of rolling elements. A more correct estimation of the hysteresis shape can find its applications in feed forward position control to avoid more complicated model structures which are computationally intensive and less appropriate for online application.

ACKNOWLEDGMENTS

This research is supported by the fund for Scientific Research-Flanders (F.W.O.) under Grant FWO4283. Professor P. Vanherck is greatly acknowledged for fruitful discussions and comments. Tegoeh Tjahjowidodo and Thierry Janssens are acknowledged for their support during the experiments. The scientific responsibility is assumed by its authors.

REFERENCES

[1] B. Armstrong-Hélouvry, *Control of Machines with Friction*, Kluwer Academic Publishers, Norwell, Mass, USA, 1991.

[2] F. Al-Bender and W. Symens, "Characterization of frictional hysteresis in ball-bearing guideways," *Wear*, vol. 258, no. 11-12, pp. 1630–1642, 2005.

[3] V. Lampaert, F. Al-Bender, and J. Swevers, "Experimental characterization of dry friction at low velocities on a developed tribometer setup for macroscopic measurements," *Tribology Letters*, vol. 16, no. 1-2, pp. 95–106, 2004.

[4] F. Al-Bender and W. Symens, "Dynamic characterization of hysteresis elements in mechanical systems—I: theoretical analysis," *Chaos*, vol. 15, no. 1, Article ID 013105, 11 pages, 2005.

[5] F. Al-Bender and W. Symens, "Dynamic characterization of hysteresis elements in mechanical systems—II: experimental validation," *Chaos*, vol. 15, no. 1, Article ID 013106, 9 pages, 2005.

[6] F. Al-Bender and K. De Moerlooze, "A model of the transient behavior of tractive rolling contacts," *Advances in Tribology*. vol. 2008, Article ID 214894, 17 pages, 2008.

[7] Q. Y. Liu, X. S. Jin, and Z. R. Zhou, "An investigation of friction characteristic of steels under rolling-sliding condition," *Wear*, vol. 259, no. 1–6, pp. 439–444, 2005.

[8] K. G. Budinski, "An inclined plane test for the breakaway coefficient of rolling friction of rolling element bearings," *Wear*, vol. 259, no. 7–12, pp. 1443–1447, 2005.

[9] H. Endo, E. Marui, N. Hasegawa, and H. Katagiri, "Transient rolling behaviour of a slider supported by two rollers," *Tribology International*, vol. 31, no. 7, pp. 377–384, 1998.

[10] J. Otsuka and T. Masuda, "The influence of nonlinear spring behavior of rolling elements on ultraprecision positioning control systems," *Nanotechnology*, vol. 9, no. 2, pp. 85–92, 1998.

[11] J. Wang, T. Hashimoto, H. Nishikawa, and M. Kaneta, "Pure rolling elastohydrodynamic lubrication of short stroke reciprocating motion," *Tribology International*, vol. 38, no. 11-12, pp. 1013–1021, 2005.

[12] L. Xiao, S. Björklund, and B. G. Rosén, "The influence of surface roughness and the contact pressure distribution on friction in rolling/sliding contacts," *Tribology International*, vol. 40, no. 4, pp. 694–698, 2007.

[13] R. D. Arnell, P. B. Davies, J. Halling, and T. L. Whomes, *Tribology Principles and Design Applications*, MacMillan, London, UK, 1991.

[14] H. L. Heathcote, "The ball bearing: in the making, under test and on service," *Proceedings of the Institute of Automotive Engineers*, vol. 15, pp. 569–702, 1921.

[15] K. L. Johnson, *Contact Mechanics*, Cambridge University Press, Cambridge, UK, 1985.

[16] V. Lampaert, "Modelling and control of dry sliding friction in mechanical systems," Ph.D. thesis, Division of Production Engineering, Machine design and Automation, Katholieke Universiteit Leuven, Leuven, Belgium, 2003.

[17] D. Tabor, *The Hardness of Metals*, Oxford University Press, Oxford, UK, 1951.

[18] F. Al-Bender, W. Symens, J. Swevers, and H. Van Brussel, "Theoretical analysis of the dynamic behavior of hysteresis elements in mechanical systems," *International Journal of Non-Linear Mechanics*, vol. 39, no. 10, pp. 1721–1735, 2004.